Supplementary Materials for

Interfollicular epidermal stem cells self-renew via autocrine Wnt signaling

Xinhong Lim, Si Hui Tan, Winston Lian Chye Koh, Rosanna Man Wah Chau, Kelley S. Yan, Calvin J. Kuo, Renée van Amerongen, Allon Moshe Klein*, Roel Nusse*

*correspondence to: rnusse@stanford.edu and Allon_Klein@hms.harvard.edu.

This PDF file includes:

Materials and Methods

Animals

Axin2-CreERT2 mice were previously described (*26*). Rainbow mice (*5*) were a gift from IL Weissman. Axin2-lacZ (*27*) were a gift from W. Birchmeier. Rosa26-lacZ (*28*), Rosa26-mTmG^{flox} mice (*29*) and β-catenin$^{\Delta ex2\text{-}6\text{-}flox/flox}$ (*30*) mice were obtained from The Jackson Laboratory. All alleles were heterozygous, except where stated. All experiments were approved by the Stanford University Animal Care and Use Committee and performed according to NIH guidelines.

Labeling and tracing experiments

All mice received a single intraperitoneal injection of 5-20mg/mL stock solutions of Tamoxifen (Tam) (Sigma) dissolved in corn oil/10% ethanol, corresponding to specific doses per gram body weight as specified below. Axin2-CreERT2/Rosa26mTmG^{flox} mice received a single dose of Tam at postnatal day 21 (P21), totaling 1mg/25g body weight. For quantitative analysis of the clonal fate of Axin2-CreERT2 expressing cells, Axin2-CreERT2/Rosa26-Rainbow mice received a single dose of Tam at P21, totaling 4mg/25g body weight.

Conditional knockout of β-catenin

Axin2-CreERT2/β-catenin$^{\Delta ex2\text{-}6\text{-}fl/+ \text{ or } -del/+}$ and mutant Axin2-CreERT2/β-catenin$^{\Delta ex2\text{-}6\text{-}fl/fl \text{ or } -fl/del}$ animals were injected with a single dose of Tam corresponding to 4mg/25g body weight at 3 weeks of age. Skins were harvested and processed for histology upon morbidity or death after 10-11 days of chase. Phenotypes were quantified by counting cells in images of between 10-20 unit areas of either control or mutant epidermises derived from 3 independent experiments. Cell counts were subject to pairwise Student t-tests.

Dkk overexpression

Three week-old Axin2-CreERT2 animals were given an intravenous injection of either Adeno-Fc or Adeno-Dkk1 at a dose of 5 x 10^8 PFU. Dkk1 overexpression was confirmed by analysis of serum and intestinal histology. Skins were harvested and processed for histology upon morbidity or death after 5-11 days of chase.

Detection of label-retaining cells

Animals were treated as previously described (*13*), with minor modifications. Axin2-CreERT2/Rosa26mTmG^{flox} animals were treated with Tam corresponding to either 1mg/25g or 4mg/25g body weight at P10 and then injected with 5-ethynyl-2'-deoxyuridine (EdU, Life Technologies) every 12 hours over 2-3 days (as specified), and harvested half a day after the final EdU dose (P12.5 or P13.5), and 70.5 days later (P82.5 or P83.5), and processed for histology and epidermal whole-mounts.

Wound experiments

Axin2-CreERT2/Rosa26-Rainbow^{flox} animals were treated with Tam at P21. Seven days later (P28), a full-thickness skin biopsy punch wound was created (2mm – plantar epidermis, 3mm – tail epidermis, 4mm – dorsal skin), and the skin was allowed to heal

till complete closure for 18-35 days (P46-53) and then harvested and processed to obtain epidermal whole-mounts (described below).

In vitro keratinocyte culture

Primary normal adult human epidermal keratinocytes (NHEK, Life Technologies) were cultured at clonal density (60 cells/cm^2) in EpiLife defined keratinocyte growth medium with EpiLife Defined Growth Supplement and Gentamicin/Amphotericin (Life Technologies) on 6-well tissue culture plates (Costar, Corning) coated with Coating Matrix protein (Life Technologies) in a 37°C incubator at 7% CO_2. Either DMSO (final concentration 0.04%, Sigma) or IWP-2 (final concentration 2 μM, Stemgent) was added to the culture medium at plating, and the medium was replaced daily with fresh medium containing these additives. At each time point, culture medium was removed, cells were rinsed with phosphate buffered saline (PBS) and then fixed with 4% paraformaldehyde (PFA) and washed and air dried. Cells per well were counted manually by bright-field microscopy on an Axiovert 200 equipped with an X10 numerical aperture (NA) 0.25 ACHROPLAN objective. For immunofluorescence, cells were fixed in 4% PFA and stored in PBS at 4°C before staining.

Real-time PCR gene expression analysis

NHEK were cultured as described above without additives for 48 h, then trypsinized using 0.025% Trypsin/EDTA (Life Technologies) and pelleted. Cells were homogenized using QIAshredder (Qiagen) and total RNA was purified using an RNeasy mini kit (Qiagen) according to manufacturer's instructions. The total RNA was reverse-transcribed using random primers (High Capacity cDNA Reverse Transcription kit, Life Technologies). Gene expression was then assayed by real-time PCR using stock Taqman Human Wnt Pathway Array Plates (Life Technologies) on an ABI 7900HT real-time PCR system. Primer sequences are available on the Life Technologies website.

X-gal staining

Tissues were harvested and fixed in 4% PFA for 1 h at 4°C, washed in PBS and detergent rinse (PBS with 2mM $MgCl_2$, 0.01% sodium deoxycholate and 0.02% NP-40 detergent), then stained in staining solution (PBS with 2mM $MgCl_2$, 0.01% sodium deoxycholate and 0.02% NP-40, 5mM potassium ferricyanide, 5mM potassium ferrocyanate and 1mg/mL X-gal) in the dark at room temperature overnight. Tissues were then washed, post-fixed in 4% PFA in PBS and processed for paraffin embedding and histology.

Histology and immunostaining

All immunofluorescence staining was performed in the dark. Cryosections were incubated in blocking buffer (2% Normal Donkey Serum, 0.2% Triton-X in PBS) at room temperature and stained with primary and secondary antibodies, then mounted in Prolong Gold with DAPI mounting medium (Life Technologies). Cell culture wells were filled with PBS and stored at 4°C prior to imaging. The following primary antibodies were used: GFP (1:1,000, Abcam), Ki67 (1:1,000, Abcam), phosphohistone-H3 (1:200, Millipore), Keratin 10 (1:2,000, Covance), Involucrin (1:200, Abcam) and Dkk3 (40 μg/ml, R&D). For specificity controls, recombinant human Wnt3a, human Dkk-3, and human Dkk-1 were used (all from R&D systems).

For EdU staining, cryosections were incubated with the reagents in the Click-iT EdU Alexa Fluor 647 Imaging Kit (Life Technologies) prepared according to manufacturer's instructions and mounted in Prolong Gold with DAPI mounting medium.

RNA in situ hybridization

Tissue sections cut at 5 μm thickness were processed for RNA in situ detection using the RNAscope 2-plex Detection Kit (Chromogenic) according to the manufacturer's instructions (Advanced Cell Diagnostics, Hayward, CA; (*31*)). RNAscope probes used were: Axin2 (NM_015732, region 330-1287), which was detected using the Fast Red detection reagent, and Wnt3 (NM_009521), Wnt4 (NM_009523, region 2147-3150), Wnt6 (NM_009526), Wnt10a (NM_009518, region 479-1948), Wnt10b (NM_011718, region 989-2133) and Dkk3 (NM_015814, region 1513-2703), which were detected using the Green detection reagent.

Epidermal whole-mountsSegments of plantar and tail skin were incubated in EDTA (5mM) diluted in PBS at 37°C for 1h. Epidermis were separated from the dermis as an intact sheet using forceps, fixed overnight and stored in 4% PFA prior to being mounted on slides in Prolong Gold with DAPI for imaging. For EdU staining of whole-mounts, tissues were washed in blocking buffer containing 3% Bovine Serum Albumin in PBS, then incubated with the reagents in the Click-iT EdU Alexa Fluor 647 Imaging Kit (Life Technologies) prepared according to manufacturer's instructions, then mounted in Prolong Gold with DAPI mounting medium and imaged.

Microscope image acquisition and quantification

All sections were imaged using the Axioplan 2 or Axiovert Imager.Z2 Microscope, the AxioCam MRm (fluorescence) and MRC5 (bright field) cameras and using Axiovision AC software (Release 4.1 and 4.8, Carl Zeiss). Image acquisitions were done at room temperature using X10 NA 0.3, X20 NA 0.5, and X40 NA 0.75 EC Plan-Neofluar objectives and X20 NA 0.8 Ph2 and X40 NA 1.3 Ph3 Apochromat objectives (Carl Zeiss). All whole-mount epidermis tissues were imaged using confocal microscopy. To quantify labeled cells during homeostasis, we acquired 1,024x1,024 pixel sequential scans at room temperature using a Leica SP5 or SP8 confocal detection system fitted on either on a Leica DM6000 upright or DMI6000 inverted microscope equipped with a X20 NA 0.75 HC PL Apochromat glycerol immersion objective, X40 NA 1.3 HCX PL Apochromat oil immersion objective (Leica) and using Leica LAS AF system software. Z-stacks were acquired at 0.6 μm depth and reconstructed using Volocity software (Improvision).

Fluorescence images of cultured cells were imaged using a Nikon Eclipse Ti-S equipped with a QImaging Retiga Exi Mono camera and a X10 NA 9.30 Plan Fluor objective. To assess the contribution of labeled cells to wound healing, we acquired 1,024x1,024 pixel sequential scans at room temperature using the Leica SP5 and SP8 confocal microscopy setups equipped with a X10 NA 0.3 HC PL Fluotar dry objective, X20 NA 0.75 HC PL Apochromat glycerol immersion objective, and X25 NA 0.95 HCX Apochromat water immersion objective (Leica) and Leica LAS AF system software.

Tiled images were stitched together in LAS AF or using the Stitching plugin (*32*) in Fiji (*33*), or Adobe Photoshop (Adobe Systems) and quantified using ImageJ (*34*).
For some images, contrast, color and dynamic range were globally adjusted in Adobe Photoshop (Adobe Systems) or in the Leica LAS AF system software. Basal and suprabasal Axin2-CreERT2-labeled cells were manually quantified either using printed confocal images or using 3-D reconstructed Z-stacks in Volocity. BrdU-labeled cells were either manually counted or automatically quantified by segmentation of single cells using CellProfiler (*35*) and custom code written in Matlab (The Mathworks, Natwick, CA). Nuclei for total cell counts were quantified using Matlab and CellProfiler. In the Matlab code, thresholding and watershed transforms were used.

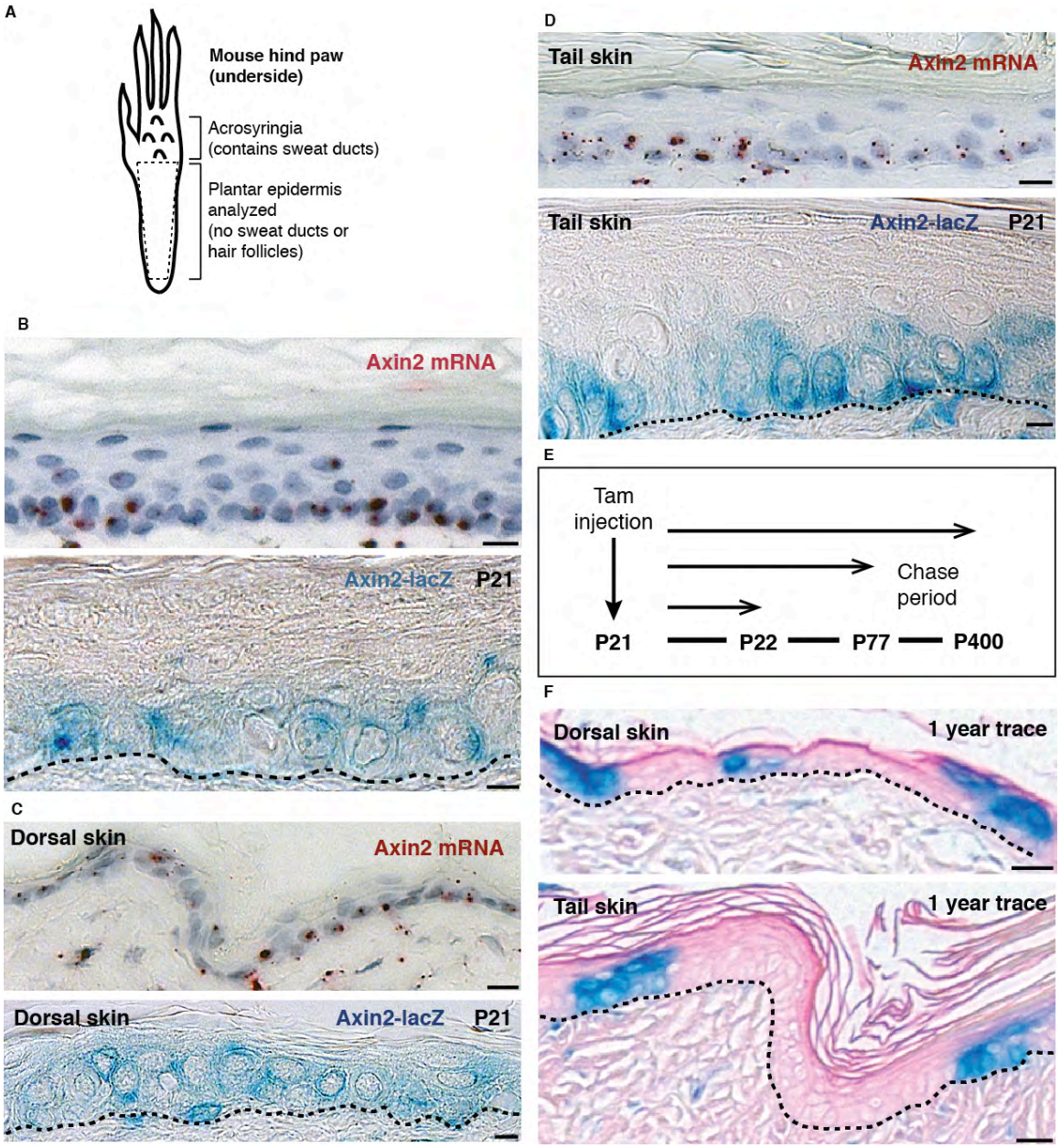

Figure S1.
Basal epidermal cells in multiple skin compartments are Axin2-expressing progenitors.
(A) Schematic of the underside of the mouse hind paw. Dashed box indicates region of plantar epidermis examined in the current study. **(B-D)** Axin2 mRNA (red spots) and Axin2-lacZ expression in 3-week old mouse **(B)** plantar, **(C)** dorsal and **(D)** tail epidermis. Dashed line denotes approximate location of epidermis/dermis boundary. Scale bars for Axin2 mRNA images, 10 μm. Scale bars for Axin2-lacZ images, 5 μm. **(E)** Schematic depicting pulse-chase experiment to track the fate of Axin2+ cells. Abbreviations: Tamoxifen (Tam), Postnatal Day 21 (P21). **(F)** To track the fate of Axin2+ cells and their progeny in postnatal skin, Axin2-CreERT2/Rosa26lacZ^{flox} mice were injected with Tamoxifen (Tam) at P16, and their skins were harvested after chasing

for one year. Clones were found to persist in dorsal and tail epidermis. Dashed lines denote approximate location of epidermis/dermis boundary. Scale bars, 10 μm.

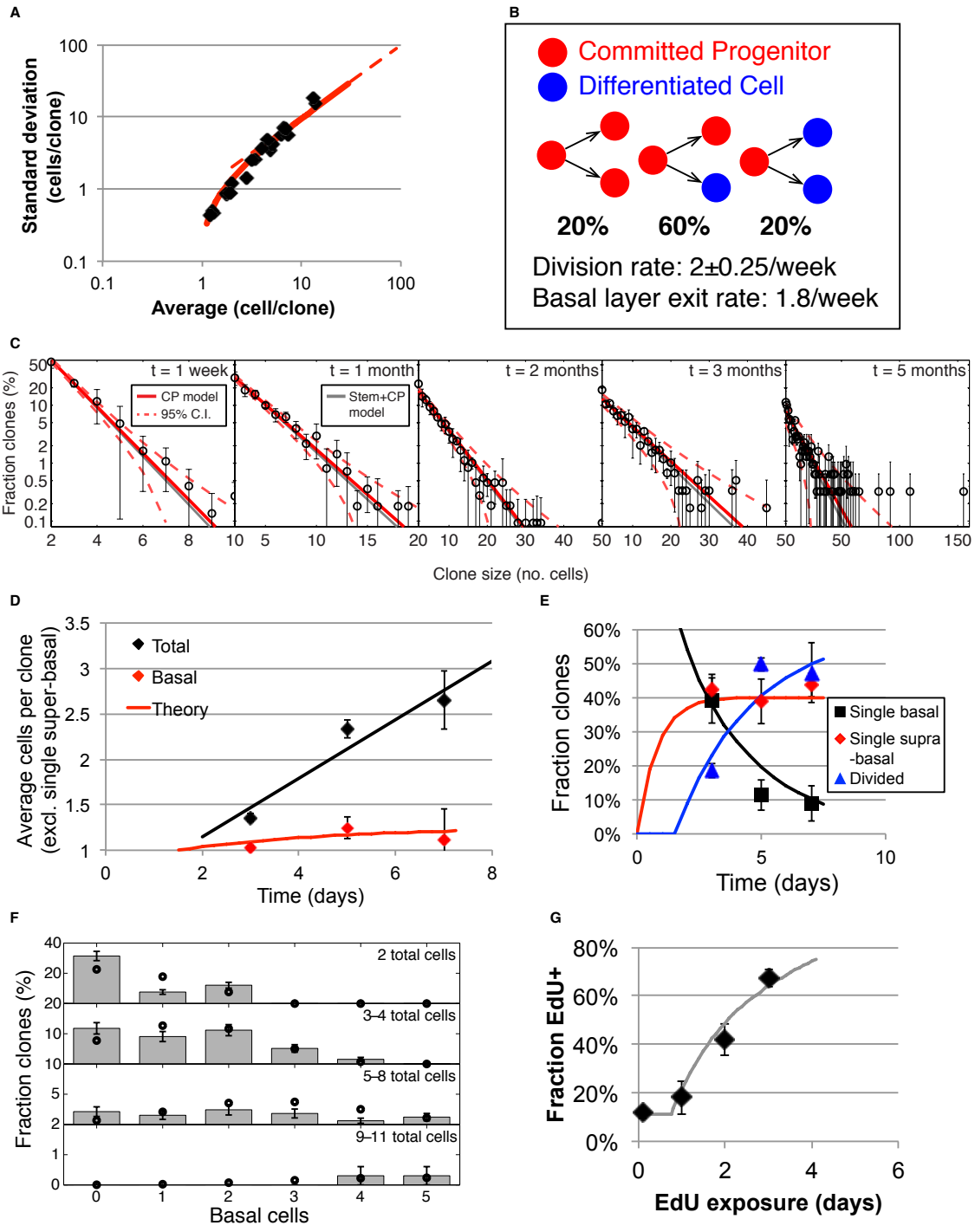
A
Standard deviation (cells/clone)
Average (cell/clone)
B
Committed Progenitor
Differentiated Cell
20%
60%
20%
Division rate: 2±0.25/week
Basal layer exit rate: 1.8/week
C
t = 1 week
t = 1 month
t = 2 months
t = 3 months
t = 5 months
CP model
95% C.I.
Stem+CP model
Fraction clones (%)
Clone size (no. cells)
D
Total
Basal
Theory
Average cells per clone (excl. single super-basal)
Time (days)
E
Single basal
Single supra -basal
Divided
Fraction clones
Time (days)
F
2 total cells
3–4 total cells
5–8 total cells
9–11 total cells
Fraction clones (%)
Basal cells
G
Fraction EdU+
EdU exposure (days)

H

Age	N	Vertical length (v)	horizontal length (h)
P22	3	0.47 cm	0.30 cm
P44	1	0.50 cm	0.35 cm
P57	2	0.50 cm	0.30 cm
P85	1	0.50 cm	0.30 cm
P111	1	0.50 cm	0.40 cm
P150	1	0.55 cm	0.35 cm
P219	1	0.50 cm	0.35 cm
P471	1	0.50 cm	0.30 cm

Figure S2.
Quantitative analysis of IFESC self-renewal by Axin2-CreERT2 lineage tracing and EdU incorporation.
(A) Clones derived from Axin2-CreERT2 labeled cells show hallmarks of neutral competition between IFESCs, with the mean and variance in clone size satisfying Taylor's law (Supplementary Theory [**ST]** S-III). **(B)** A probabilistic 'committed progenitor' (CP) cell model of cell fate that gives rise to neutral IFESC competition ((*8*); **ST** S-IV). In this model, the CP cells act as the functional IFESCs. More complex models may also generate the same hallmarks of neutral competition (Stem+CP model (*10*)) and generate similar quality fits (**ST** S-VI). Since all of these models involve cells competing neutrally, we refer to them as Neutral Competition (NC) models. **(C)** Distribution in the number of basal layer cells per clone over 5 months post-labeling (error bars = SD, n=3 mice). Red curve shows fit to the model of probabilistic cell fate shown in (B) (CP model); solid grey curve shows fit assuming the presence of rare, slow-cycling stem cells (Stem+CP model) (**ST** S-VI); dashed curves show 95% confidence intervals of fit. **(D-F)** High temporal resolution, short-time clone dynamics are consistent with same NC models of IFESC cell fate that fit the long-term data (see **ST** S-V). **(D)** The average number of cells per clone (total = basal + suprabasal cells) grows linearly with a mean cell division rate of 2.25/week (black curve). The average number of basal cells per clone (red) has a near-constant value over time as expected by the model shown in (B) (**ST** S-V). Note that the basal layer data differs from that in Fig. 1D, which shows only persisting clones (containing at least two cells in the basal layer); here the plot shows the true basal layer average clone size, including clones with zero basal layer cells but at least two suprabasal layer cells. **(E)** The first fate choice of Axin2-CreERT2 labeled cells. Single labeled cells undergo direct suprabasal migration (red), or division (blue) or remain undivided in the basal layer (black). The curves show the NC model fit (**ST** S-V). **(F)** The same model fits the joint distribution in the number of basal and suprabasal cells per clone at 7 days post-

labeling (**ST** S-V). Circles show theory predictions (error bars = SD, n=3 mice). **(G)** Independent estimation of the cell division rate by ongoing EdU incorporation over 3 days (**Methods**). The fit (grey curve) is consistent with a division rate $\lambda=2.2\pm0.2$/week, and with IFESCs occupying a fraction $\rho=0.8\pm0.1$ of the basal layer (see **ST** S-I). **(H)** Dimensions of mouse plantar epidermis at different ages during the period of analysis. N denotes number of mice measured at each age. The analyzed region does not change in size over the duration of the study.

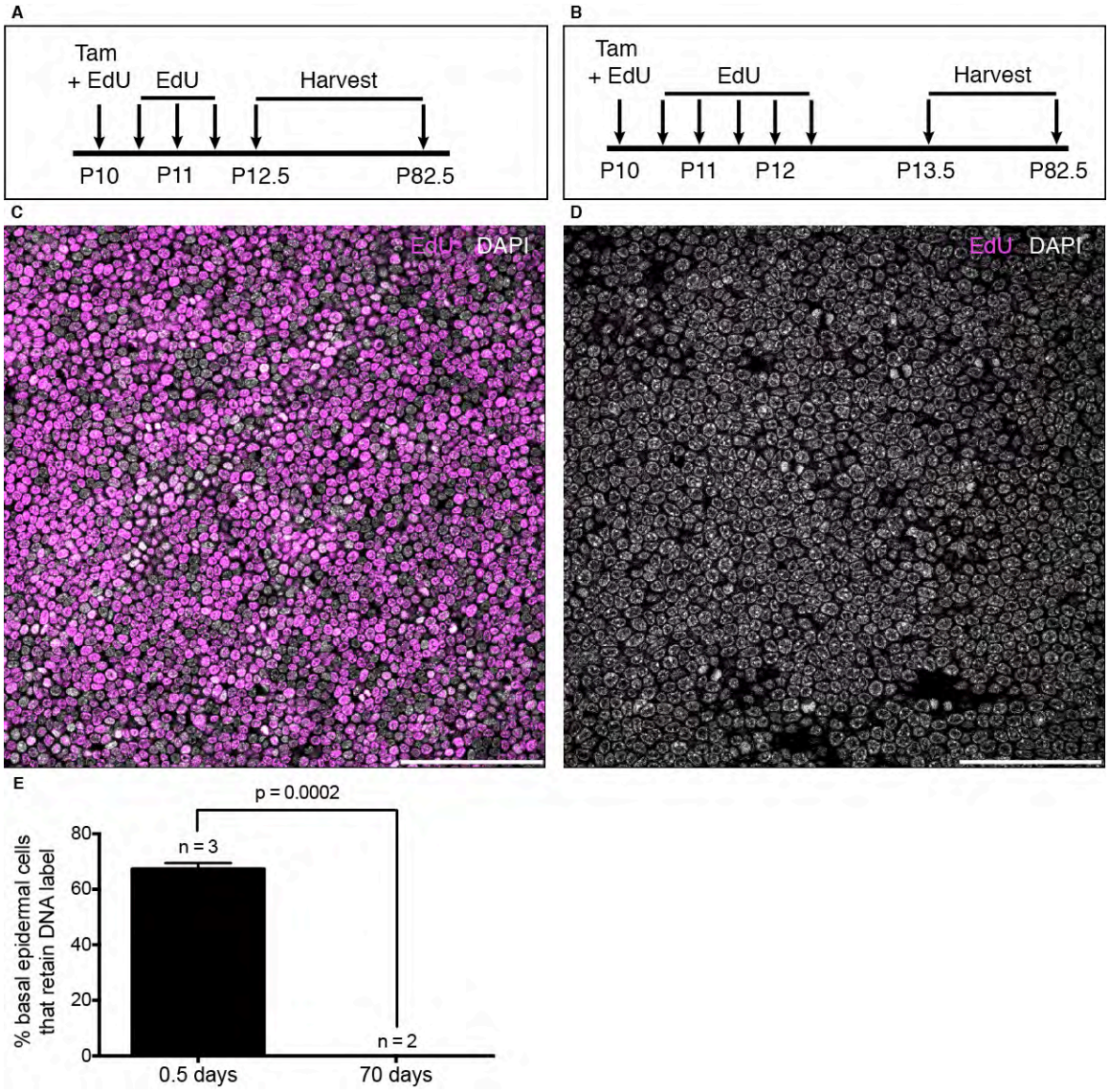

Figure S3.
EdU label-retention in plantar epidermis.
(A,B) Schematic depicting Tamoxifen and EdU pulse-chase experiment to detect label-retaining Axin2-CreERT2-labeled cells in **(A)** sections (48h EdU) and **(B)** epidermal whole-mounts (72h EdU). **(C-D)** Representative whole-mount confocal images of plantar basal epidermis chased for **(C)** 0.5 days (P13.5) and **(D)** 70.5 (P83.5) days are shown. Scale bars, 100 μm. **(E)** Changes in the proportion of EdU+ basal cells as determined by counting and plotting EdU+ nuclei of plantar epidermal whole-mounts (error bars = SEM). N denotes the number of animals examined at each timepoint.

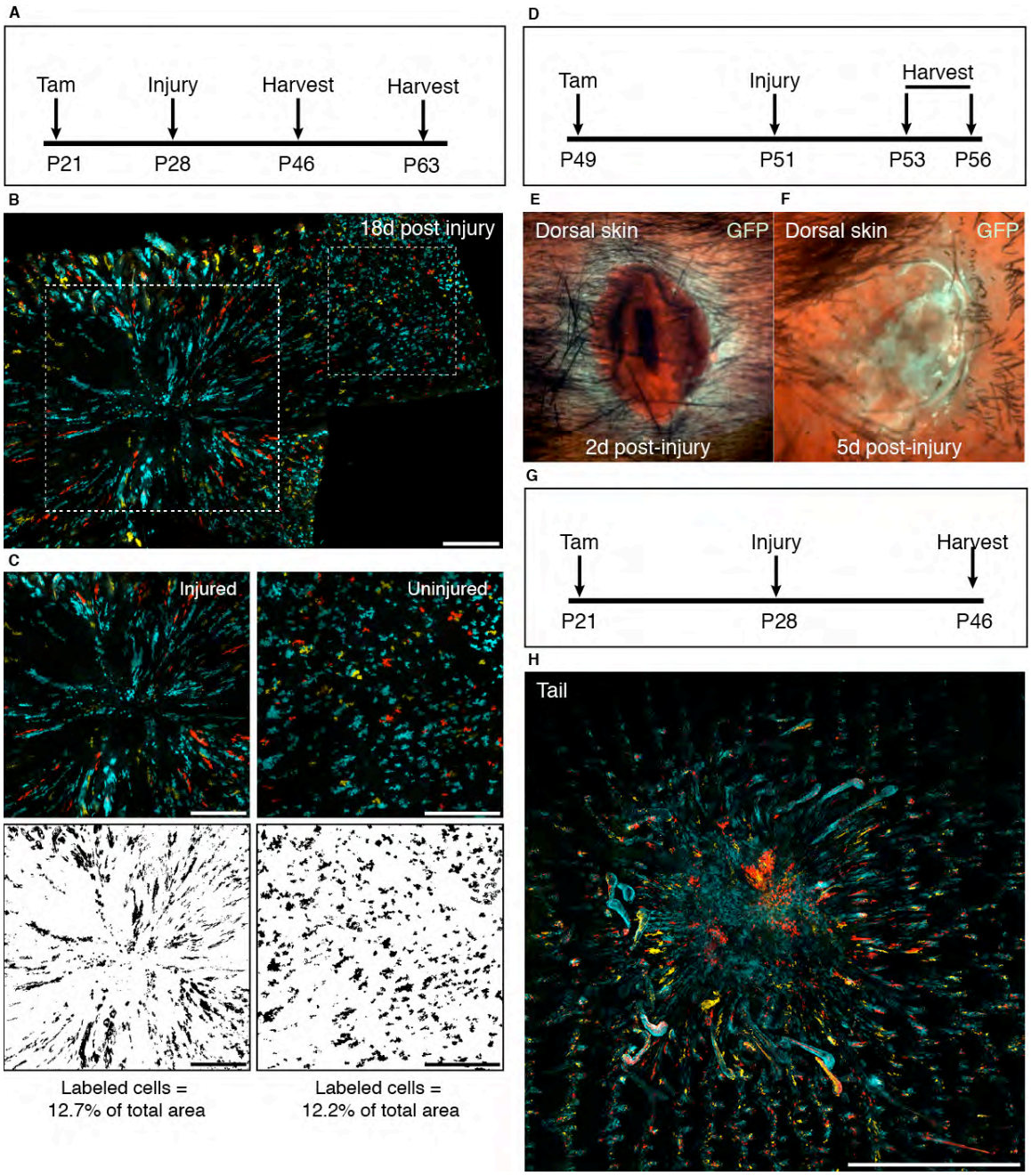

Figure S4.
Contribution of Axin2-CreERT2-labeled cells to epidermal wound healing.
(A) Schematic depicting experiment to determine contribution of Axin2-CreERT2-labeled cells to healing skin. **(B)** Whole-mount views of healing Axin2-CreERT2/Rosa26-Rainbow^{flox} plantar epidermis at 18-days post-wounding. Dashed squares denote approximate injured (left) and uninjured (right) areas. **(C)** Enlarged view and image masks of injured and uninjured area denoted by dashed squares in (B). Scale bars, 300 µm. **(D)** Schematic depicting experiment to determine contribution of Axin2-CreERT2-labeled cells to healing dorsal skin. **(E,F)** Whole-mount view of healing Axin2-CreERT2/Rosa26mTmG^{flox} dorsal skin at **(E)** 2 days and **(F)** 5 days post-injury.

(G) Schematic depicting experiment to determine contribution of Axin2-CreERT2-labeled cells to healing Axin2-CreERT2/Rosa26-Rainbow^{flox} tail skin. **(H)** Whole-mount view of healing tail skin at 18 days post-injury. Scale bar, 2.50 mm.

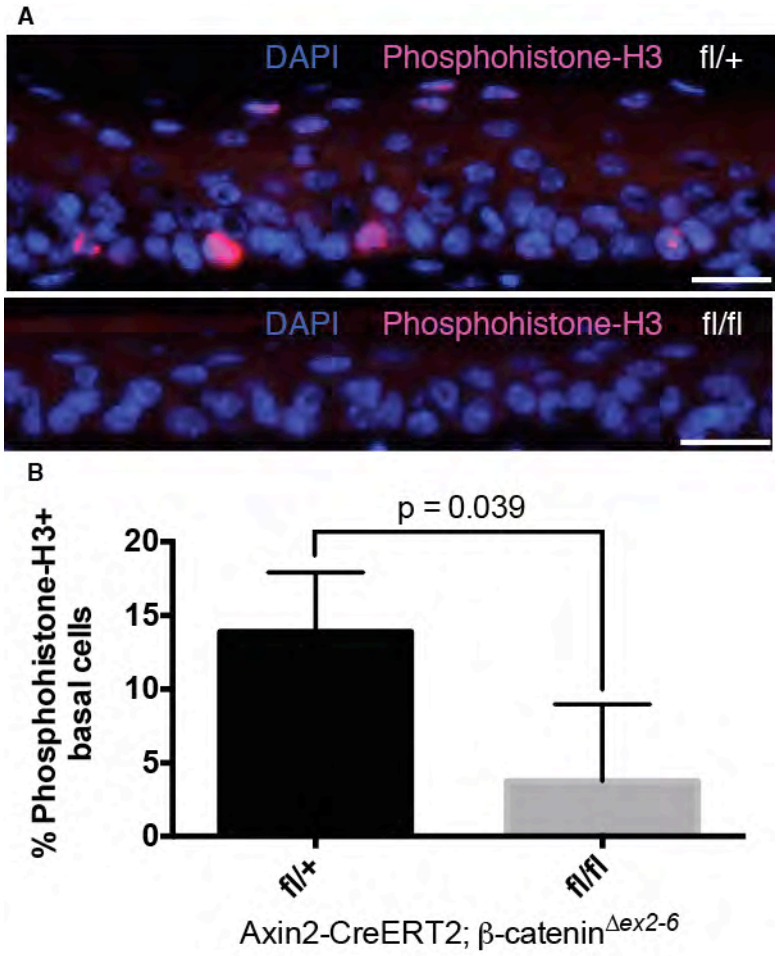

Figure S5.
Axin2-expressing interfollicular epidermal stem cells require β-catenin to proliferate.
(A) Representative images of phosphohistone-H3 immunostaining of control Axin2-CreERT2/β-catenin$^{\Delta ex2\text{-}6\text{-}fl/+ \text{ or } -del/+}$ and mutant Axin2-CreERT2/β-catenin$^{\Delta ex2\text{-}6\text{-}fl/fl \text{ or } -fl/del}$ plantar epidermis. Scale bars, 10 μm. **(B)** Changes in proliferative index between control and mutant plantar epidermises as determined by counting and plotting phosphohistone-H3+ nuclei in the basal layer. All counts were derived from n>=3 independent experiments and subject to pairwise Student t-tests.

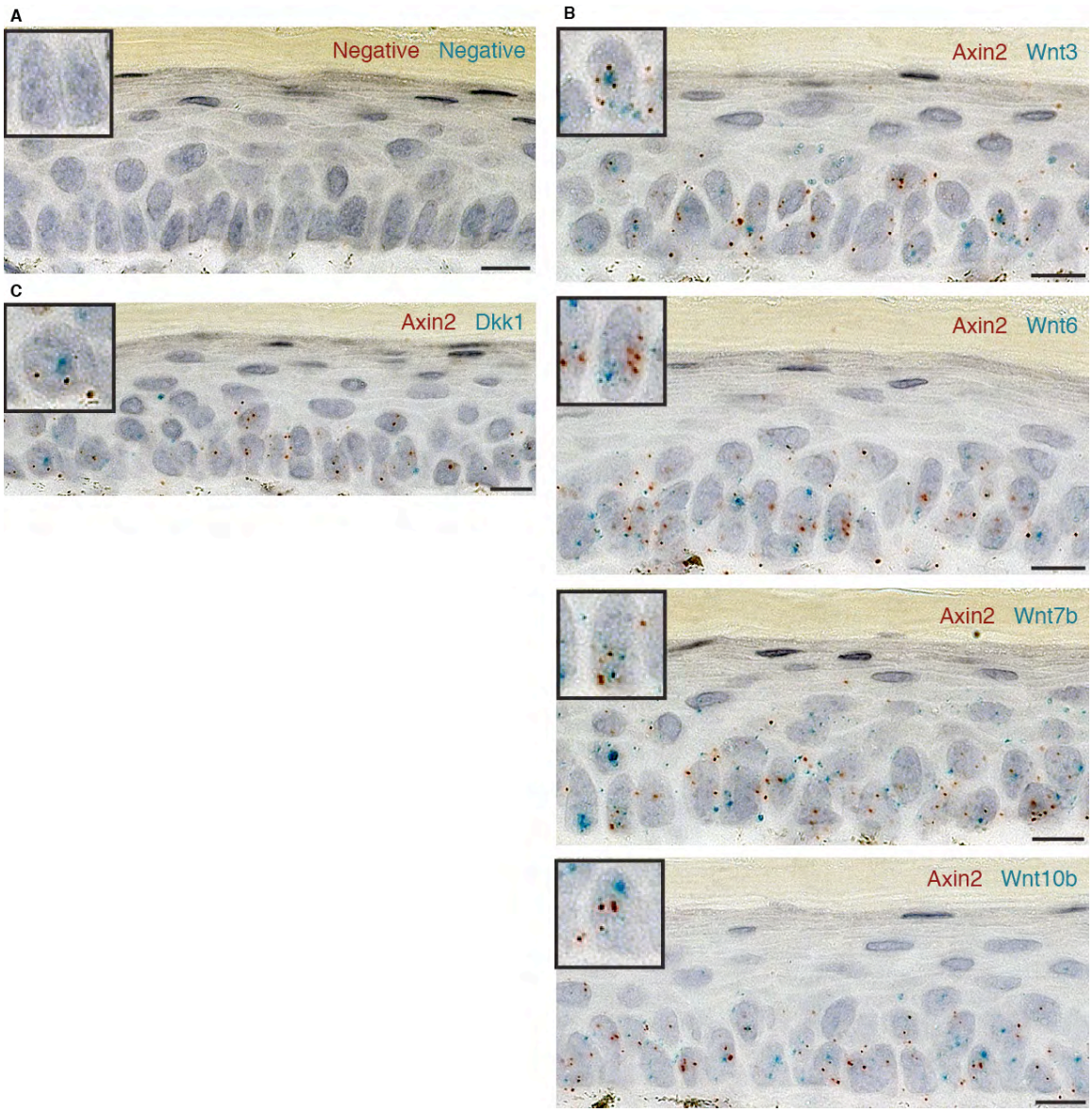

Figure S6.
Axin2-expressing interfollicular epidermal stem cells express Wnt and Wnt inhibitors.
(A-C) Representative images of double-labeling RNA *in situ* hybridization in mouse plantar epidermis for expression of **(A)** bacterial DapB (negative control), **(B,C)** Axin2 (red spots) and **(B)** Wnt3, Wnt6, Wnt7b,Wnt10b (turquoise spots), **(C)** and Dkk1 (turquoise spots). Inset boxes show magnified view of individual basal cells expressing both Axin2 and Wnts/Dkk. Scale bars, 10 μm.

Gene	C_t Values				
	Run 1	Run 2	Run 3	Average	STDEV
HPRT1	27.95	27.95	27.96	27.96	0.01
CTNNB1	26.96	25.95	25.95	26.28	0.58
FZD6	27.93	27.96	27.95	27.95	0.01
GSK3B	26.90	26.93	26.92	26.92	0.01
TCF7L1	27.97	27.95	27.96	27.96	0.01
TCF7L2	31.99	30.93	30.91	31.28	0.62
PORCN	27.92	27.93	27.94	27.93	0.01
DKK1	24.96	24.95	24.95	24.95	0.00
DKK3	26.99	26.98	26.97	26.98	0.01
SFRP1	29.99	28.95	28.95	29.29	0.60
SFRP4	N.D.	N.D.	N.D.	N.D.	N.D.
WNT1	N.D.	N.D.	N.D.	N.D.	N.D.
WNT2	N.D.	N.D.	N.D.	N.D.	N.D.
WNT4	36.97	36.97	35.97	36.64	0.58
WNT5B	28.96	28.96	28.97	28.96	0.00
WNT7A	26.94	26.94	26.95	26.94	0.01
WNT7B	29.94	30.01	28.97	29.64	0.58
WNT10A	33.97	33.97	33.95	33.96	0.01
WNT10B	34.95	34.95	34.96	34.95	0.00
FGF4	N.D.	N.D.	N.D.	N.D.	N.D.
PITX2	N.D.	N.D.	N.D.	N.D.	N.D.

Figure S7.
Gene expression by primary normal adult human epidermal keratinocytes
Table of cycle threshold (C_t) values obtained using Taqman realtime RT-PCR probes on total RNA obtained from primary normal adult human epidermal keratinocytes cultured in defined medium. HUGO gene symbols are displayed. All assays were run in technical triplicates. C_t values ≤ 29 are considered to indicate abundant target nucleic acid in the sample, and C_t values between 30-37 indicate moderate amounts of target nucleic acid in the sample. N.D. = not detected.

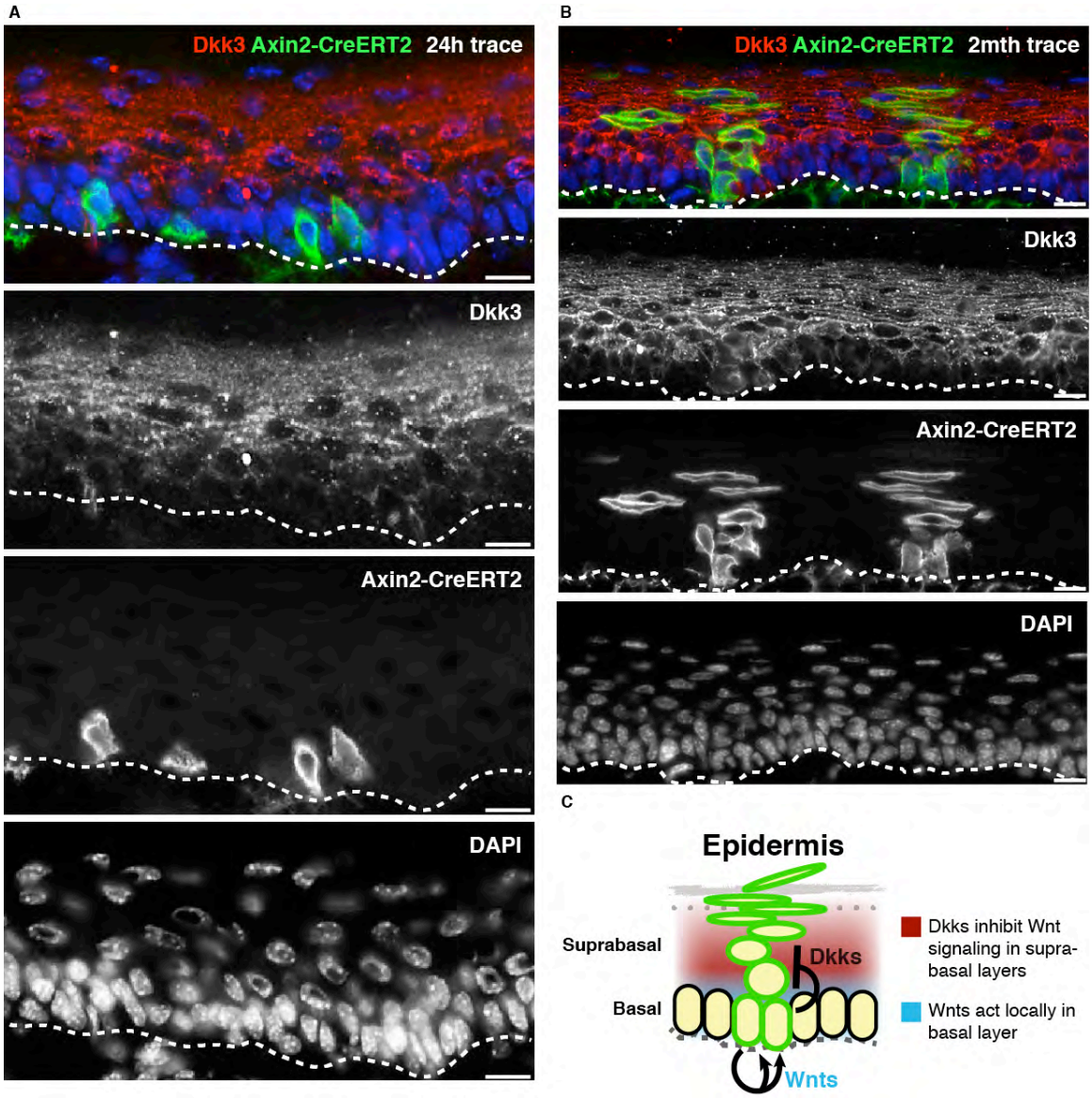

Figure S8.
Dkk3 protein is localized to the suprabasal epidermal layers, adjacent to Axin2-CreERT2-labeled IFESCs.
Representative images and separate color channels of Dkk3 immunostaining in plantar epidermises of Axin2-CreERT2/Rosa26mTmG^{flox} mice exposed to Tam at P21 and chased for **(A)** 1-day (P22) and **(B)** 2 months (P77). Scale bars, 10 µm. **(C)** Model depicting Wnt secretion by IFESCs inducing autocrine Wnt/β-catenin signaling, and simultaneous production of the longer-range Dkk inhibitor to suppress Wnt signaling in their differentiated progeny.

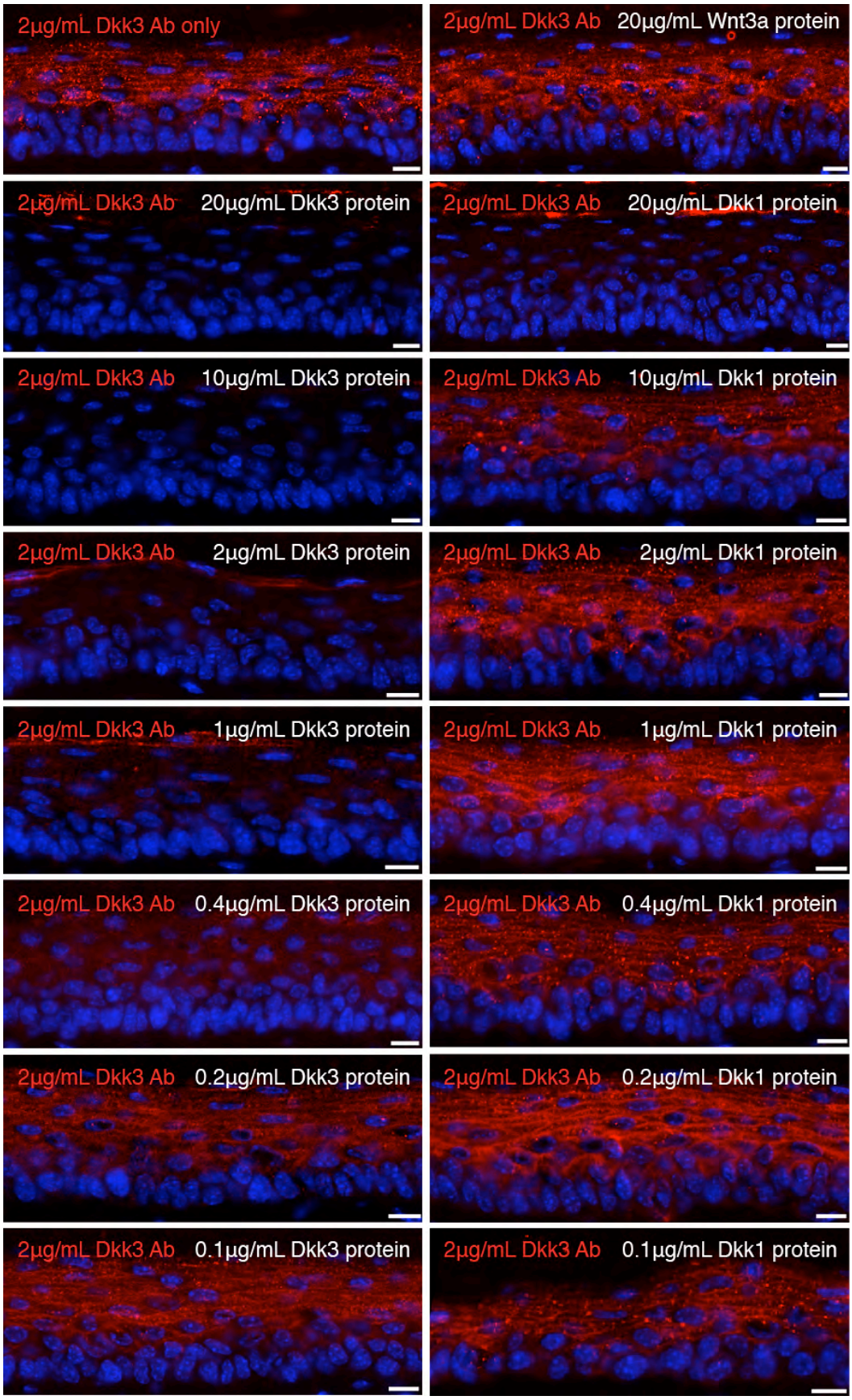
2µg/mL Dkk3 Ab only
2µg/mL Dkk3 Ab 20µg/mL Wnt3a protein
2µg/mL Dkk3 Ab 20µg/mL Dkk3 protein
2µg/mL Dkk3 Ab 20µg/mL Dkk1 protein
2µg/mL Dkk3 Ab 10µg/mL Dkk3 protein
2µg/mL Dkk3 Ab 10µg/mL Dkk1 protein
2µg/mL Dkk3 Ab 2µg/mL Dkk3 protein
2µg/mL Dkk3 Ab 2µg/mL Dkk1 protein
2µg/mL Dkk3 Ab 1µg/mL Dkk3 protein
2µg/mL Dkk3 Ab 1µg/mL Dkk1 protein
2µg/mL Dkk3 Ab 0.4µg/mL Dkk3 protein
2µg/mL Dkk3 Ab 0.4µg/mL Dkk1 protein
2µg/mL Dkk3 Ab 0.2µg/mL Dkk3 protein
2µg/mL Dkk3 Ab 0.2µg/mL Dkk1 protein
2µg/mL Dkk3 Ab 0.1µg/mL Dkk3 protein
2µg/mL Dkk3 Ab 0.1µg/mL Dkk1 protein

Figure S9.
Specificity controls for Dkk3 antibody staining.
Representative images of Dkk3 immunostaining in plantar epidermises of Axin2-CreERT2/Rosa26mTmG^{flox} mice exposed to Tam at P21 and chased for 1 or 2 months. Labeled clones are not shown. Skin sections were incubated with either 2 μg/mL of Dkk3 antibody alone, or 2 μg/mL of Dkk3 antibody with various concentrations of human Wnt3a, Dkk3, or Dkk1 protein to compete with the tissue for antibody binding. Scale bars, 10 μm. The Dkk3 antibody may bind with low affinity to Dkk1 protein, since Dkk1 can compete for antibody binding when added at high concentrations (10-fold protein or 20 μg/mL Dkk1) but not at lower concentrations. In contrast, up to 10-fold less added Dkk3 protein (0.2 μg/mL Dkk3) can compete for Dkk3 antibody binding, suggesting that Dkk3 antibody binds with much higher specificity to Dkk3 protein.

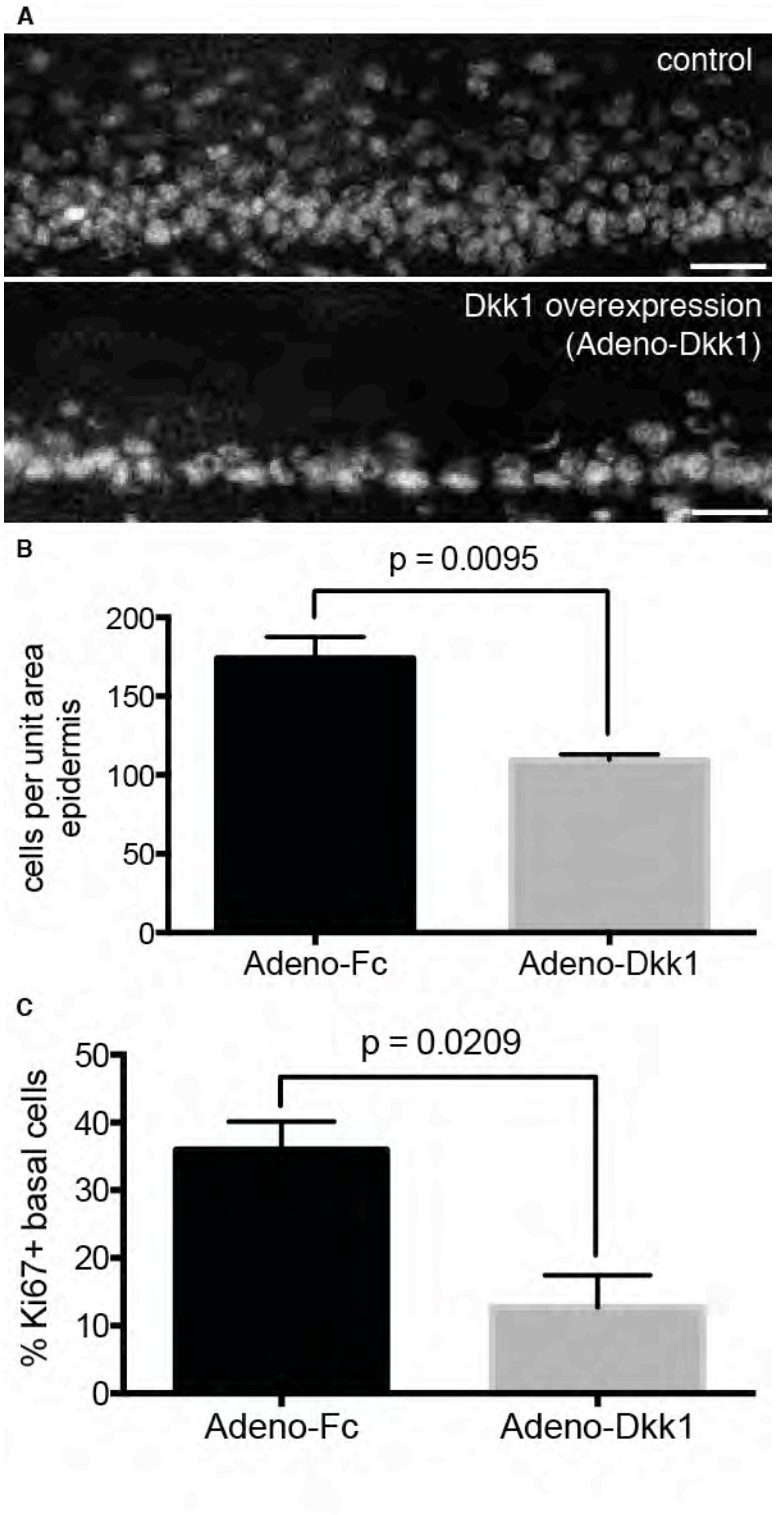

Figure S10.
Dkk1 overexpression induces epidermal thinning.
(A) Representative images of DAPI-stained plantar epidermises from Adeno-Fc (control) and Adeno-Dkk1 treated Axin2-CreERT2 mice. **(B,C)** Changes in cellularity and

proliferative index between control and mutant plantar epidermises as determined by counting and plotting **(B)** DAPI+ and **(C)** Ki67+ nuclei in the basal layer (error bars = SEM). All counts were derived from n=3 independent experiments and subject to unpaired Student t-tests. Scale bars, 20 μm.

Supplementary theory and data analysis

Here we describe the methods used for quantitative analysis of cell fate in homeostatic turnover of the mouse paw epidermis. Our analysis is based on models of stochastic fate choice that have been validated through a number of studies (*8,10*), (*36*), and reviewed in (*11*). For the reader's convenience we reproduce here the key results, referring the reader to the literature for more theoretical details.

S-I Evaluation of cell cycle time from EdU incorporation kinetics

S-I.1 Theory

In this experiment, mice are treated with consecutive pulses of EdU over a time interval t, giving a fraction of EdU-labeled basal layer cells $[\text{EdU\%}](t)$. The average cell cycle time of progenitor cells can be evaluated from the rate of increase in $[\text{EdU\%}](t)$, according to a method proposed in Ref. (*10*). Here we make a minor adjustment to the original method, which holds only in the case where the entire basal layer consists of progenitor cells (i.e. cells fated to undergo division). We extend the analysis to the case where a fraction $0 < \rho < 1$ of the basal layer consists of progenitors, while the remaining cells are post-mitotic cells fated to migrate supra-basally.

Following (*10*) we denote as f_{S} the fraction of the cell cycle a progenitor cell spends in S phase, and λ the average division rate. The fraction of progenitor cells that have taken up EdU after a time t of continuous EdU incorporation is given approximately by,

$$p(t) = 1 - (1 - f_{\text{S}})e^{-\lambda t}\,.$$

This expression is exact if the progenitor cell cycle distribution is exponentially distributed. For each progenitor cell that divides, on average, a post-mitotic cell must detach from the basal layer. The labeled post-mitotic fraction is therefore found to be,

$$m(t) = 1 - e^{-\rho\lambda t/(1-\rho)}\,.$$

Together, the fraction of all basal layer cells that are labelled by EdU after a time t is,

$$\begin{aligned}[\text{EdU\%}](t) &= \rho\, p(t) + (1-\rho)\, m(t) \\ &= 1 - \rho\,(1 - f_{\text{S}})\, e^{-\lambda t} - (1-\rho)e^{-\rho\lambda t/(1-\rho)}\,.\end{aligned}$$

Finally, noting that $[\text{EdU\%}](0) = \rho f_{\text{S}}$ is the fraction of labeled basal layer cells following a single EdU pulse, we obtain the fitting equation,

$$[\text{EdU\%}](t) = 1 - [\rho - [\text{EdU\%}](0)]\, e^{-\lambda t} - (1-\rho)e^{-\rho\lambda t/(1-\rho)}\,. \qquad \text{(S1)}$$

S-I.2 Fit to data

The division rate λ was estimated by fitting Eq. (S1) to the fraction of EdU$^+$ cells (Supp. Fig. 2G) using a non-linear least-squares algorithm implemented in MATLAB. The fit requires additionally estimating the progenitor cell fraction ρ. In addition, since the injection of Tamoxifen appears to induce a pause in cell cycle entry (see Supp. Fig. 2G), we introduce a lag time $t_0 = 0.75$ days, which reflects a period of cell cycle suppression at the start of the experiment. The fraction $[\text{EdU\%}](0)$ from a single EdU pulse was measured to be $12 \pm 2\%$. To test sensitivity of λ to the estimated value of ρ, we performed the fit over a range of ρ values. The fitted value of λ varied little with the precise choice of ρ for $\rho > 0.5$, giving a range $\lambda = 2.1$-2.6/week.

S-II Evaluation of clonality of labeled cells in Axin2-CreERT2/Rosa26-Rainbow lineage tracing experiments

Following Tamoxifen treatment of Axin2-CreERT2/Rosa26-Rainbow mice, only a small fraction of cells are labelled with mCherry (RFP) or mOrange (mOr); the remaining labeled cells express mCerulean (CFP). The average fraction of cells labeled in each color remains constant throughout the five months chase period. All clonal analysis was performed on RFP and mOr cells, since the low labeling frequency in these colors suggests that contiguous patches of RFP or mOr cells are likely to be clonal. To test this assumption, we used the incidence of contact between clones of two colors (RFP and mOr) to calculate the fraction of single-color patches that might result from contact between two clones of the same color. For this calculation, we assume that clone color is chosen at random with no spatial bias, an assumption that can be confirmed from the uniform spatial distribution of clones in low magnification images. We also assume that contact between three or more clones is negligible owing to the low labeling frequency. With these assumptions, if we count x_1 RFP clones in an experiment, x_2 mOr clones, and x_{12} occurrences in which an RFP clone is in direct contact with a mOr clone, then the fraction of single-color patches that are poly-clonal can be estimated to be,

$$f_{\text{contact}} \simeq \frac{1}{2} \frac{x_{12}}{x_1 + x_2} \left(\frac{x_2}{x_1} + \frac{x_1}{x_2} \right) . \tag{S2}$$

This approximation holds provided that $f_{\text{contact}} \ll 1$. Applying Eq. (S2), we calculated that 98-99.8% of all contiguous groups of mOr and RFP labeled-cells are in fact monoclonal, viz. $f_{\text{contact}} = 0.9 \pm 0.7\%$ (mean$\pm$SD), with a range $0.2 - 1.9\%$ between different mice ($N = 10$, see Table S1).

Table S1: Calculation of clone collision fractions for a sample of 10 mice.

Mouse	Time	x_1	x_2	x_{12}	f_{contact}
XH739	3 days	290	194	2	0.45%
XH741	3 days	688	372	17	1.92%
XH796	5 days	622	891	27	1.90%
XH710	1 week	446	698	11	1.06%
XH726	1 week	306	538	9	1.24%
XH720	1 month	975	1501	28	1.24%
HT196	1 month	757	1001	4	0.24%
XH686	2 months	1064	1755	16	0.64%
XH578	5 months	443	1133	2	0.19%
XH579	5 months	1223	1971	8	0.28%

S-III Hallmarks of neutral competition in Axin2-CreERT2/Rosa26-Rainbow lineage tracing experiments

S-III.1 Theory

Although the clones traced in Axin2-CreERT2/Rosa26-Rainbow mice all originate from single cells labeled concurrently, the distribution in the number of basal layer cells per clone at later times becomes increasingly heterogeneous (Supp. Fig. 2C). A central goal of quantitative clonal analysis is to predict the observed heterogeneity in clone sizes based on models of stem cell behavior (*37*).

Before fitting the data to any particular model of stem cell behavior, we perform a general classification of the tissue self-renewal strategy based on the clonal dynamics, as detailed in (*11*). Since the labeled cells maintain a constant cell population in homeostasis (Fig. 1E), the rates of division and differentiation of the cells must be precisely balanced. This may occur through invariant asymmetric division of stem cells, ensuring that each division gives rise to one stem cell and a second daughter cell that is fated to differentiate. Alternatively, the stem cell pool may self-renew through a combination of asymmetric divisions with population asymmetric self-renewal, in which basal layer progenitor cells may divide symmetrically or differentiate (*37*). In the former case, each long-lived clone is self-sustaining, supported by a single stem cell. In the latter case, each clone may either expand or shrink in size in a stochastic manner as a result of symmetric divisions and stem cell differentiation. Since the total number of stem cells remains constant in homeostasis, the result of population asymmetry is that clones effectively `compete' with one clone expanding while a neighboring clone contracts. Neutral competition leaves several characteristic features in the clonal size distributions, which are summarized below.

1. The tissue is maintained by an ever decreasing clonal population of ever increasing size: Following Ref. (*8*), we define a □surviving clone□ as one that maintains at least one basal layer cell. Population asymmetric self-renewal leads the fraction of surviving clones to decrease hyperbolically with time, $P_{\text{surv.}}(t) \sim 1/t$, while the average number of cells in surviving clones grows linearly to compensate for the drop in clone number, $\langle n(t) \rangle_{\text{surv.}} \sim t$.

2. Clone sizes become increasingly heterogeneous over time, with the variance satisfying Taylor's Law: Taylor's law states that the variance in clone size is a power-law of the average, viz (*38*)

$$\text{Var}[n(t)]_{\text{surv.}} = C \times \left(\langle n(t) \rangle_{\text{surv.}}\right)^{\alpha} .$$

In the long-time limit neutral competition between clones leads to Taylor's law with a constant pre-factor $C = 1$ and an exponent $\alpha = 2$. At earlier times post-labeling, Taylor's law holds only approximately and we expect a fit with $\alpha > 1$.

3. Scaling of clone size distributions: As discussed in Ref. (*11*), the neutral competition between clones causes the long-term clone size distribution to asymptote to a `scaling' form in which the chance of finding a clone larger than some multiple of the average becomes constant. Formally, this scaling behavior is expressed as

$$\lim_{\lambda t \to \infty} P_n(t) = F\left(n / \langle n(t) \rangle_{\text{surv.}}\right) ,$$

where $P_n(t)$ is the fraction of surviving clones hosting at least n basal layer cells. The `scaling function' $F(x)$ has a universal form that is independent of the detailed regulation in the tissue. In a laminar (two-dimensional) tissue such as the epidermis, we expect $F(x) = e^{-x}$.

S-III.2 Data analysis

The clone size data show all of the qualitative and quantitative hallmarks of population asymmetric self-renewal and neutral clonal competition. Figures 1C, D show the number of surviving clones and their average size; Supp. Fig. 2A shows that the clone sizes satisfy Taylor's law; and Supp. Fig. 2C shows that the clone size distributions indeed fit the predicted universal scaling curve with exponential profile. We may therefore conclude that, with each division, some fraction of stem cells differentiate while the persisting stem cells multiply to replace those that are lost. The clones stochastically expand and contract, leading to a predictable drop in clone numbers. Neutral competition results in winners as well as losers: the surviving clones expand ensuring that the total number of stem cells remains constant.

S-IV The Committed Progenitor (CP) cell model

S-IV.1 Model definition

Since the clone fate data shows hallmarks of population asymmetric self-renewal, we used a model combining symmetric and asymmetric cell divisions to analyze the data, first described in (*8*), (*36*). This model attributes the entire self-renewal potential of the basal layer to a single population of `committed progenitors' (or CP cells). Since the CP cells are capable of self-renewing indefinitely as a population, they are a functional stem cell population. With each division, the CP cells give rise at random to either two daughter progenitor cells, two post-mitotic cells, or one progenitor and one post-mitotic cell. Denoting CP cells as type A, basal layer post-mitotic cells as type B, and supra-basal cells as type C, the model consists of a Markov process with the following rules,

$$\begin{aligned} \mathrm{A} &\xrightarrow{\lambda} \begin{cases} \mathrm{A}+\mathrm{A} & \text{Prob. } r \\ \mathrm{A}+\mathrm{B} & \text{Prob. } 1-2r \\ \mathrm{B}+\mathrm{B} & \text{Prob. } r \end{cases} \\ \mathrm{B} &\xrightarrow{\Gamma} \mathrm{C} \end{aligned} \tag{S3}$$

Here the mean division rate is λ, the migration rate from the basal layer to the supra-basal layers is Γ, and the probability of symmetric division is $2r$. Since the size of the labeled cell population remains constant, the probabilities of symmetric division leading to clone expansion (A$\rightarrow$2A) and clone contraction (A$\rightarrow$2B) are equal. In terms of these parameters, the fraction of basal cells that are progenitors fated to divide is $\rho = \Gamma/(\Gamma+\lambda)$. The remaining fraction $(1-\rho)$ will exit the basal layer to be replaced by the division of nearby cells.

To relate the model to data, we solve the Master Equation associated with (S3) to obtain the clone size distribution, $P_{n_\mathrm{A},n_\mathrm{B},n_\mathrm{C}}(t)$, which gives the probability of finding a clone with n_A progenitor cells, n_B post-mitotic basal layer cells, and n_C supra-basal layer cells at a time t after Tamoxifen treatment. We refer the reader to Refs. (*36*, *39*) for the form of the Master Equation and its solution.

S-IV.2 Fit of the CP cell model to basal layer clone size distributions

At long times, only the number of basal cells is tracked, so for process (S3) we calculate the fraction of clones with n basal layer cells, viz.

$$P_n(t) = \sum_{n_A=0}^{\infty}\sum_{n_B=0}^{\infty}\sum_{n_C=0}^{\infty} P_{n_\mathrm{A},n_\mathrm{B},n_\mathrm{C}}(t)\delta_{n,n_\mathrm{A}+n_\mathrm{B}} \,,$$

where $\delta_{n,m}$ is the Kroenecker delta function. Since only clones with $n \geq 1$ basal cells can be tracked, we fit the model to the data through the surviving clone size distribution, $P_n^{(\text{surv.})}(t) = P_n(t)/[1 - P_0(t)]$.

We take the division rate to be $\lambda = 2.2$/week, as estimated from the rate of EdU incorporation (see above). To determine the values of ρ and r consistent with the data, we first solve the Master Equation (*36*, *39*) to obtain the predicted $P_n^{(\text{surv.})}(t)$ for a range of parameter values spanning $0 < \rho < 1$ and $0 < r < 1/2$. (Note that the migration rate is $\Gamma = \lambda/(1/\rho - 1)$). The Likelihood of each parameter combination ($\rho,\ r$) is then calculated from the data to obtain a maximum Likelihood estimate of the parameters,

$$\mathcal{L}(\rho, r) \propto \prod_{j=1}^{N_m} \prod_{k=1}^{N_j} P_{n_{j,k}}^{(\text{surv.})}(t_j - t_0)\,, \tag{S4}$$

where $N_m = 21$ is the number of mice analyzed; N_j clones were scored for mouse j, t_j gives the time point for the j-th mouse, and $n_{j,k}$ gives the number of basal cells scored in the k-th clone for the j-th mouse. The parameter t_0 reflects a pause in cell division that occurs following Tamoxifen induction; since this pause is short, it can be neglected for fits at times $t \geq 1$ week. Three mice were scored for each of seven time points, totaling 10,053 clones in total with N_j ranging between 115 and 1,167 clones per mouse. The parameter Likelihoods (not shown) indicating that the data is consistent with a range of possible values for ($r,\ \rho$), constrained to the parameter sub-space $\rho = 0.13 + 3.3r$ with $r \geq 0.1$. For $\rho = 0.8 \pm 0.1$ (estimated below from short-time analysis), the best fit corresponds to $r = 0.2 \pm 0.03$.

S-V Testing for a short-term bias in the fate of Axin2$^+$ progenitor cells

At 3, 5 and 7 days post-labeling, we score both basal and supra-basal cells per clone. (At later times the supra-basal cells enter the cornified layer, where they lose their nucleus and can no longer be scored). This data can be analyzed for possible short-term biases in cell fate choice, which only later regress to the balanced stochastic fate seen in the long-term data. To test for potential bias, we attempt to fit the data to a `null model' in which there is *no* short-term bias in cell fate. According to this model, the first progenitor cell division after labeling precisely follows the probabilistic outcomes of the CP cell model (S3). By contrast, if the model derived for the long-time behavior fails to fit the short-time data, this may indicate a bias in cell fate resulting from active Wnt signaling in Axin2-CreERT2 labeled cells.

Analysis of the model (S3) reveals several predictions for the stochastic model: first, the average number of cells per clone (including both basal and supra-basal cells) is predicted to grow linearly, with a division rate reflecting the tissue average, viz.

$$\langle n(t) \rangle_{\text{tot.}} = 1 + \lambda(t - t_0) \qquad \text{for } t \geq t_0\,. \tag{S5}$$

Here the parameter t_0 reflects a pause in cell cycle resulting from Tamoxifen application. Fitting Eq. (S5) to the data in Supp. Fig. 2D, we find that the data is consistent with $\lambda = 2.25$/day and $t_0 = 1.5$ days. These values show a somewhat longer pause in cell cycle for labeled cells compared to that found by EdU incorporation in unlabeled cells (section S-I), but is consistent with a lower fraction of EdU incorporation in Axin2-CreERT2 labeled cells in the first 24 hours post-labeling compared to the unlabeled cells. The division rate agrees well with that inferred for the entire cell population through continuous EdU labeling.

Second, the average number of basal cells per clone can be calculated for progenitor cell-derived clones, now including `extinct' clones that contain zero basal cells. We find for the null model,

$$\langle n(t)\rangle_{\text{basal}} = 1 + \left(\frac{1}{\rho} - 1\right)\left(1 - e^{-\Gamma(t-t_0)}\right) \qquad \text{for } t \geq t_0\,. \tag{S6}$$

Note that with λ and t_0 fit above, Eq. (S6) has just a single free parameter, ρ, because $\Gamma = \lambda/(1/\rho - 1)$. A fit of Eq. (S6) to the data in Supp. Fig. 2D (red curve) reveals $\rho = 0.8 \pm 0.1$, meaning that the supra-basal migration rate of post-mitotic cells is extremely rapid, $\Gamma = 1.3 \pm 0.2$/day.

Third, we study the fraction of clones consisting of exactly two supra-basal cells and no basal cells. From the model solution for the clone size distribution $P_{n_{\rm A},n_{\rm B},n_{\rm C}}(t)$, we calculate the predicted fraction of clones with n basal layer cells and m supra-basal layer cells, viz.

$$P_{n,m}(t) = \sum_{n_A=0}^{\infty}\sum_{n_B=0}^{\infty} P_{n_{\rm A},n_{\rm B},m}(t)\delta_{n,n_{\rm A}+n_{\rm B}}\,.$$

To focus on progenitor cell behavior, we analyze clones with at least two cells, defining,

$$P^{(\text{exp.})}_{n,m}(t) = \frac{P_{n,m}(t)}{1 - P_{0,0}(t) - P_{0,1}(t) - P_{1,0}(t)} \qquad \text{for } n + m \geq 2\,. \tag{S7}$$

With these definitions, the model predicts $P^{(\text{exp.})}_{0,2}(t) \to r$, and we find that the data is consistent with this behavior with $r = 26 \pm 3\%$ (Supp. Fig. 2F, $N = 3$ mice), in close agreement to the value of r found from the long-term fits.

These fits indicate that the short-time clonal evolution is consistent with the same stochastic model seen in the long-time data. Indeed, solving the Master Equation with the parameters $\rho = 0.8$, $r = 0.25$, $\lambda = 2.25$/week and $t_0 = 1.5$ days, Supp. Fig. 2F shows that the entire joint distribution of the number of basal and supra-basal cells per clone is fit by the stochastic model (S3) at 3, 5 and 7 days post-labeling.

S-VI Searching for slow-cycling stem cells in plantar IFE

The CP cell model (S3) provides an excellent fit to the clone fate data in this and earlier papers (*8,9*), (*40*), suggesting that just a single, rapidly cycling progenitor cell occupies the basal layer of the epidermis and acts as a functional stem cell compartment. However, could the same observations be consistent with a different model of tissue maintenance, whereby a population of slow-cycling stem cells replenishes the rapidly-cycling CP cells that form the majority of the basal layer? Such a model, which predicts the same hallmarks of neutral competition found in our data (section S-III), was proposed in a recent paper studying mouse tail skin homeostasis (*10*). In particular, to reconcile the presence of slow-cycling cells with ongoing neutral competition, it was proposed that rare, slow-cycling, stem cells also follow a probabilistic fate outcome similar to that described in (S3) (for a full definition of the model, see (*10*). Each stem cell was proposed to divide approximately 4-6 times per year. Upon wounding, the stem cells become activated and contribute to tissue regeneration.

We tested whether the presence of slow-cycling stem cells was consistent with our experimental results in plantar epidermis. First, assuming that slow cycling stem cells are present, we determined whether Axin2-CreERT2 labeling might enrich for them, or alternatively exclude them. Since the fraction of labeled cell in the basal layer remains constant over time (Fig. 1E), we concluded that, if slow-cycling stem cells exist, they are neither enriched nor depleted in the labeled population. Consistent with this, both Axin2-CreERT2 labeled and unlabeled cells contribute equally wound healing (Fig. 2B, Supp Fig. 4C).

Second, we estimated the maximum fraction of basal layer cells that might be slow-cycling. Following Axin2-CreERT2 labeling, only 9% of clones consisted of a single basal layer cell after one week (Supp. Fig. 2E), imposing an upper bound on the slow-cycling cell fraction. For a stricter upper bound, we turned to the EdU label-retention assay (Fig. 1F,G, Supp. Fig. 3). In this experiment, if a fraction ρ_{S} of all basal layer cells are slow-cycling with an average division rate λ_{S}, then the labeled slow-cycling cells represent a fraction $[\mathrm{EdU}\%] = \rho_{\mathrm{S}}\lambda_{\mathrm{S}}T_{\mathrm{pulse}}$ of all cells in the basal layer, where $T_{\mathrm{pulse}} = 3$ days is the duration of the EdU pulse (and $\lambda_{\mathrm{S}}T_{\mathrm{pulse}} \ll 1$). Following 70 days, we find $[\mathrm{EdU}\%] = 0.025\%$ ($N = 141,588$ cells), from which we may estimate that the fraction of cells with a cell cycle time longer than 2.5 months is $\rho_{\mathrm{S}} \approx (0.03/\mathrm{year})/\lambda_{\mathrm{S}}$. Thus, if $\lambda_{\mathrm{S}} = 4$/year as proposed in (*10*), they cannot constitute more than $\rho_{\mathrm{S}} = 0.75\%$ of cells in the basal layer of plantar epidermis. Conversely, if the slow-cycling stem cells occupy 5% of the IFE as proposed in (*10*), they must remain almost entirely inactive in normal homeostasis, dividing approximately once every 1.5 years --- i.e. just twice during the entire lifetime of the mouse.

Third, we assessed whether slow cycling stem cells would be detectable in our clone fate data. Using the estimate $\rho_{\mathrm{S}} = 5\%$ and $\lambda_{\mathrm{S}} = 4$/year, we fit the hierarchical model proposed in (*10*) as described therein. This choice of parameters over-estimates the activity of slow-cycling stem cells by approximately 6-fold (as determined above from the product

$\rho_S\lambda_S$). Nevertheless, even with this over-estimate, there is no significant difference in the quality of fits assuming the absence or presence of slow-cycling stem cells (solid red and grey curves respectively in Supp. Fig. 2C). Thus, if present, the slow cycling stem cells do not significantly alter clone fate, and consequently they play little or no role in normal tissue homeostasis.

In conclusion, while the clone fate data result from Axin2-CreERT2 labeling cannot rule out the presence of very slow cycling stem cells in mouse plantar IFE, we may conclude that they are either very rare, or extremely quiescent, and consequently they do not contribute significantly to tissue homeostasis over the time scale of mouse adult life. Moreover, since a large fraction of Axin2-CreERT2 labeled clones contribute to wound healing (Fig. 2 and Supp Fig. 4), we may conclude that regeneration, as well as normal tissue maintenance, cannot be attributed to rare slow-cycling cells.

References

1. J. Huelsken, R. Vogel, B. Erdmann, G. Cotsarelis, W. Birchmeier, beta-Catenin controls hair follicle morphogenesis and stem cell differentiation in the skin, *Cell* **105**, 533–545 (2001).

2. S. Beronja *et al.*, RNAi screens in mice identify physiological regulators of oncogenic growth, *Nature* **501**, 185–190 (2013).

3. H. Snippert *et al.*, Lgr6 Marks Stem Cells in the Hair Follicle That Generate All Cell Lineages of the Skin, *Science* **327**, 1385 (2010).

4. V. P. Losick, L. X. Morris, D. T. Fox, A. Spradling, Drosophila stem cell niches: a decade of discovery suggests a unified view of stem cell regulation, *Developmental Cell* **21**, 159–171 (2011).

5. H. Ueno, I. L. Weissman, Clonal Analysis of Mouse Development Reveals a Polyclonal Origin for Yolk Sac Blood Islands, *Developmental Cell* **11**, 519–533 (2006).

6. I. C. Mackenzie, Relationship between Mitosis and the Ordered Structure of the Stratum Corneum in Mouse Epidermis, *Nature* **226**, 653–655 (1970).

7. C. S. Potten, The epidermal proliferative unit: the possible role of the central basal cell, *Cell Tissue Kinet* **7**, 77–88 (1974).

8. E. Clayton *et al.*, A single type of progenitor cell maintains normal epidermis, *Nature* **446**, 185–189 (2007).

9. D. P. Doupé, A. M. Klein, B. D. Simons, P. H. Jones, The ordered architecture of murine ear epidermis is maintained by progenitor cells with random fate, *Developmental Cell* **18**, 317–323 (2010).

10. G. Mascre *et al.*, Distinct contribution of stem and progenitor cells to epidermal maintenance, *Nature* (2012), doi:10.1038/nature11393.

11. A. M. Klein, B. D. Simons, Universal patterns of stem cell fate in cycling adult tissues, *Development* **138**, 3103–3111 (2011).

12. J. R. Bickenbach, J. McCutecheon, I. C. Mackenzie, Rate of Loss of Tritiated Thymidine Label In Basal Cells In Mouse epithelial tissues, *Cell Prolif* **19**, 325–333 (1986).

13. K. M. Braun *et al.*, Manipulation of stem cell proliferation and lineage commitment: visualisation of label-retaining cells in wholemounts of mouse epidermis, *Development* **130**, 5241–5255 (2003).

14. S. Reddy *et al.*, Characterization of Wnt gene expression in developing and postnatal

hair follicles and identification of Wnt5a as a target of Sonic hedgehog in hair follicle morphogenesis, *Mechanisms of Development* **107**, 69–82 (2001).

15. F. Witte, J. Dokas, F. Neuendorf, S. Mundlos, S. Stricker, Comprehensive expression analysis of all Wnt genes and their major secreted antagonists during mouse limb development and cartilage differentiation, *Gene Expression Patterns* **9**, 215–223 (2009).

16. N. Radoja, A. Gazel, T. Banno, S. Yano, M. Blumenberg, Transcriptional profiling of epidermal differentiation, *Physiol. Genomics* **27**, 65–78 (2006).

17. Y. Yamaguchi *et al.*, Mesenchymal-epithelial interactions in the skin: increased expression of dickkopf1 by palmoplantar fibroblasts inhibits melanocyte growth and differentiation, *J Cell Biol* **165**, 275–285 (2004).

18. G. Du *et al.*, Expression of REIC/Dkk-3 in normal and hyperproliferative epidermis, *Exp Dermatol* **20**, 273–277 (2011).

19. H. Schlüter, H.-J. Stark, D. Sinha, P. Boukamp, P. Kaur, WIF1 Is Expressed by Stem Cells of the Human Interfollicular Epidermis and Acts to Suppress Keratinocyte Proliferation, *J Invest Dermatol* (2013), doi:10.1038/jid.2013.42.

20. I. del Barco Barrantes *et al.*, Generation and Characterization of dickkopf3 Mutant Mice, *Molecular and Cellular Biology* **26**, 2317–2326 (2006).

21. J. J. Barrott, G. M. Cash, A. P. Smith, J. R. Barrow, L. C. Murtaugh, Deletion of mouse Porcn blocks Wnt ligand secretion and reveals an ectodermal etiology of human focal dermal hypoplasia/Goltz syndrome, *Proc Natl Acad Sci USA* (2011), doi:10.1073/pnas.1006437108.

22. W. Liu *et al.*, Deletion of Porcn in Mice Leads to Multiple Developmental Defects and Models Human Focal Dermal Hypoplasia (Goltz Syndrome), *PLoS ONE* **7**, e32331 (2012).

23. J. L. Bolognia, J. L. Jorizzo, J. V. Schaffer, in *Dermatology*, (Mosby-Saunders, London, 2012), pp. 869–885.

24. H. Nguyen *et al.*, Tcf3 and Tcf4 are essential for long-term homeostasis of skin epithelia, *Nat Genet* **41**, 1068–1075 (2009).

25. Y. S. Choi *et al.*, Distinct functions for Wnt/beta-catenin in hair follicle stem cell proliferation and survival and interfollicular epidermal homeostasis, *Cell Stem Cell* (2013).

26. R. van Amerongen, A. N. Bowman, R. Nusse, Developmental Stage and Time Dictate the Fate of Wnt/β-Catenin-Responsive Stem Cells in the Mammary Gland, *Cell Stem Cell* (2012), doi:10.1016/j.stem.2012.05.023.

27. B. Lustig *et al.*, Negative feedback loop of Wnt signaling through upregulation of

conductin/axin2 in colorectal and liver tumors, *Molecular and Cellular Biology* **22**, 1184–1193 (2002).

28. P. Soriano, Generalized lacZ expression with the ROSA26 Cre reporter strain, *Nat Methods* **21**, 70–71 (1999).

29. M. D. Muzumdar, B. Tasic, K. Miyamichi, L. Li, L. Luo, A global double-fluorescent Cre reporter mouse, *Genesis* **45**, 593–605 (2007).

30. V. Brault *et al.*, Inactivation of the beta-catenin gene by Wnt1-Cre-mediated deletion results in dramatic brain malformation and failure of craniofacial development, *Development* **128**, 1253–1264 (2001).

31. F. Wang *et al.*, RNAscope, *The Journal of Molecular Diagnostics* **14**, 22–29 (2012).

32. S. Preibisch, S. Saalfeld, P. Tomancak, Globally optimal stitching of tiled 3D microscopic image acquisitions, *bioinformatics.oxfordjournals.org*.

33. J. Schindelin *et al.*, Fiji: an open-source platform for biological-image analysis, *Nat Methods* **9**, 676–682 (2012).

34. C. A. Schneider, W. S. Rasband, K. W. Eliceiri, NIH Image to ImageJ: 25 years of image analysis, *Nat Methods* **9**, 671–675 (2012).

35. L. Kamentsky *et al.*, Improved structure, function and compatibility for CellProfiler: modular high-throughput image analysis software, *Bioinformatics* **27**, 1179–1180 (2011).

36. A. M. Klein, D. P. Doupé, P. H. Jones, and B. D. Simons, ``Kinetics of cell division in epidermal maintenance," Phys. Rev. E, vol. 76, p. 021910, 2007.

37. B. D. Simons and H. Clevers, ``Strategies for homeostatic stem cell self-renewal in adult tissues.," Cell, vol. 145, pp. 851--862, June 2011.

38. L. R. Taylor, ``Aggregation, Variance and the Mean," Nature, vol. 189, pp. 732--735, Mar. 1961.

39. T. Antal and P. L. Krapivsky, ``Exact solution of a two-type branching process: clone size distribution in cell division kinetics," Journal of Statistical Mechanics: Theory and Experiment, vol. 07, p. 028, July 2010.

40. A. M. Klein, D. E. Brash, P. H. Jones, and B. D. Simons, ``Stochastic fate of p53-mutant epidermal progenitor cells is tilted toward proliferation by UV B during preneoplasia.," Proceedings of the National Academy of Sciences of the United States of America, vol. 107, pp. 270--275, Jan. 2010.